Modulating Force of Nucleated Hydrogen Bubble Adhesion to Boost Electrochemical Water Splitting

Jaysri Das[a,§], Subhankar Mandal[b,§], Angana Borbora,[a] Sonam Rani,[a] Mizuki Tenjimbayashi[d]* Uttam Manna[a,b,c*]

[*][a] Department of Chemistry, Indian Institute of Technology Guwahati, Assam, 781039 India

E-mail: umanna@iitg.ac.in

[b] Centre for Nanotechnology, Indian Institute of Technology Guwahati, Assam 781039 India

[c] Jyoti and Bhupat Mehta School of Health Science & Technology, Indian Institute of Technology Guwahati, Assam, 781039 India,

[*][d] Research Center for Materials Nanoarchitectonics (MANA), National Institute for Materials Science (NIMS), Tsukuba, Ibaraki, Japan E-mail: TENJIMBAYASHI.Mizuki@nims.go.jp

Abstract

In electrochemical hydrogen evolution reaction (HER), the produced hydrogen gas bubbles often adhered to the electrode surface—and blocked the active catalytic site. While different catalysts were developed to improve the catalytic performance of HER, the design of a durable and universal approach for minimizing the force of nucleated hydrogen gas-bubble adhesion to prevent blockage of electrocatalytic sites because of bubbles-adhesion—is unprecedented. Generally, buoyancy should outweigh the capillary force to remove nucleated bubbles, which means these forces ratio, Eötvös number Eo > 1. Herein, we report a chemically reactive multilayer coating on an electrode to chemically modulate the adhesion force of nucleated gas-bubble on the electrode. A dual modified coating on Ni-foam provided a non-adhesive superaerophobicity with nucleated bubble adhesion force of 4.6 ± 0.3 μN—and displayed superior HER performance with lower overpotential (333 to 250 mV) at 100 mA cm^{-2} with respect to bare Ni-foam. The chemically-modulated low bubble-adhesion facilitated the early removal of nucleated tiny hydrogen gas bubbles with a minimum size of 0.64 mm and Eo = 0.05 to keep catalytic sites available for superior electrochemical HER. Such a positive impact of the prepared coating was also noted for various other electrodes.

Introduction

Electrochemical water splitting for hydrogen evolution reaction (HER) has emerged as one of the promising approaches to attend sustainable and decarbonized technology in the quest of green and renewable energy.[1-3] In this context, a humongous attention is paid to improve electrocatalytic HER through designing efficient and stable catalytic systems—including single atomic and di-atomic.[4-11] Although such catalytic systems are promising to generate more hydrogen bubbles—but they fail to address another important aspect of blockage of the catalytic sites because of the unavoidable adhesion of nucleated hydrogen bubbles.[12-13] During electrocatalysis, the generated hydrogen bubbles mostly adhered to the electrode surface until the gas bubbles grow in size to achieve enough buoyancy force to overcome the force of adhesion of generated gas bubbles on the electrode. Thus, the adhesion of generated hydrogen gas bubbles leads to the formation of a 'gas blanket' around the electrode—reducing the effective catalytic surface area—which results in an increase in ohmic and concentration overpotentials and loss of energy.[14-15] In addition, a strong bubble adhesion may likely to impose mechanical stress—which may cause exfoliation of the deposited state of art catalysts from the electrode.[16-17] Thus, to address these critical and relevant challenges, a simple and universal approach is essential to precisely modulate the force of adhesion of generated hydrogen bubbles on the electrode for uninterrupted and early removal of generated hydrogen gas.

In the past, distinct strategies were introduced to overcome the challenge of bubble attachment on the electrode, where either i) external energy was employed in different forms—including shear flow of the electrolyte,[18] acoustic field,[19] magnetic field,[20] capillary feeding[21] or ii) bubble wettability on the electrode was modulated through optimizing the surface roughness (nano/micro topography).[22-23] Out of these two general strategies, the latter approach is energy efficient and promising. For example, a MoS_2 nanosheet architecture,[24] patterned heterostructure of Co-Ni phosphide/spinel oxide,[5] pine-shaped Pt nanoarrays[25] and Ni/NiO-MoO_3-x nano array[26] that displayed superhydrophilicity and superaerophobicity (underwater), provided improved HER performance. Although these seminal reports demonstrated efficient water splitting activity, such strategies are material-specific, often require complex and harsh fabrication processes, and state-of-the-art fabrication strategies to control nano/microstructure, making them difficult to scale up for practical application. Thus, a universal strategy is required for the early detachment of gas-bubbles from gas evolving electrode surfaces.

Recently, in a rare attempt, Bae and coworkers reported a porous hydrophilic polyethyleneimine cross-linked hydrogel coating via Schiff-base condensation to impart superaerophobicity to the underlying electrode.[27] The superaerophobic hydrogel coated on nickel foam (NF) showed an improved current density (1200 mA cm^{-2}) and overpotential of -607 mV (at a current density of 500 mA cm^{-2}) with an electrochemical stability of 20 h. However, in general, such hydrogel is susceptible to mechanical stress during repetitive gas bubble detachment and chemical degradation under harsh chemical conditions. Moreover, in the past, only superaerophobicity was explored in the early detachment of generated gas bubbles, however, in reality, the force of bubble adhesion—competes with buoyancy force, which primarily controls the bubble detachment phenomenon. Hence, we hypothesize that the design of an interface with the ability to directly and precisely modulating the force of bubble adhesion on electrodes would be an alternative approach to achieve improved and unperturbed HER performance—but such a strategy is yet to be introduced in the literature.

Here, we report a chemically reactive multilayer coating (denoted as RMC) on an electrode surface (i.e. NF)—following a facile, scalable and substrate-independent layer-by-layer (LbL) deposition process through 1,4-conjugate addition reaction between amine and acrylate groups at ambient conditions as shown in Scheme 1A-B. Adequate single and dual post-covalent modifications of the RMC with selected modifiers allowed to tailor both wettability and force of gas bubble adhesion, as shown in Scheme 1C. A series of aerophobic coatings with the modulated force of the nucleated bubble adhesion from 100.3 ± 3.2 μN to 4.6 ± 0.3 μN were prepared through simple chemical modification of RMC with different types (cationic, anionic and neutral) of small hydrophilic molecules, where the enhanced surface free energy because of selected chemical modification improves the hydration of porous coating. An optimized coating with a minimum force of bubble adhesion allowed an early detachment of generated gas bubbles from the electrode surface, as shown in Scheme 1D. Tiny nucleated hydrogen gas bubbles (0.64 mm) left the coated electrode surface with negligible buoyancy force, and eventually provided a facile basis to enhance the HER performance in comparison to bare NF and other recently reported materials (Scheme 1E; more details are provided in Table S1).[12,22,27-30] An overpotential value of -39 mV (at 10 mA cm^{-2}) and high current density of 1270 mA cm^{-2} (at -0.9 V) were successfully achieved. The strategy also depletes the overpotential from -748 mV to -512 mV at high current density (at 500 mA cm^{-2}). Such positive impact on HER performance was noticed for other electrodes (carbon cloth, carbon paper etc.) as well. Thus, the current approach provided a facile and universal remedy for the early detachment of nucleated gas bubbles at gas evolving electrodes.

Results and Discussion

1. Preparation of Porous and Reactive Multilayer Coating

To design a universal and durable coating with the ability to modulate the adhesion force of nucleated hydrogen gas bubbles for their early detachment from an electrode surface, a widely accepted, simple and substrate-independent LbL deposition approach is adopted here.[31,32,33] In this purpose, the reaction mixture of branched polyethyleneimine (BPEI) and dipentaerythritol penta-acrylate (5Acl) that provides dispersion of polymeric nanocomplex (PNC) through 1,4-conjugate addition reaction was selected as one of the two deposition solutions (where another deposition solution was BPEI) to prepare multilayer (20 bilayers, each layer consist of consecutive deposition of BPEI polymer and PNC) coating on a NF electrode by following a covalent LbL deposition process.[34,35] To minimize the pore blockage of the selected porous substrate because of the deposited multilayer coating, a series of reaction mixtures were prepared, where the volume ratios of BPEI (50 mg mL^{-1}) and 5Acl (132.5 mg mL^{-1}) were gradually varied from 1:5 to 1:15 (v/v). During the multilayer construction process, the selection of volume ratio controlled the growth of the PNC, as evident from the dynamic light scattering (DLS) study in Figure 1A. Such a strategy helps to minimize the blockage of pores of the selected substrate during the LbL deposition process (Figure 1B-C). The optical microscopic/field emission scanning electron microscopic (FESEM) image analysis confirmed that the selection of the volume ratio of reactants (BPEI and 5Acl) in the reaction mixture during LbL deposition influenced the porosity and pore size of the NF electrode (Figure S1, Supporting Information). The average pore sizes and porosity were gradually increased from 96.9 ± 1.13 μm to 190.2 ± 0.67 μm and 4.3 ± 1.5 % to 16.3 ± 0.78%, respectively, on changing the composition of the reactants from 1:5 to 1:15 (v/v) as shown in Figure S2 (Supporting Information). This is likely due to the slower growth of PNC in the reaction mixture having volume ratios of 1:10 and 1:15, which prevented the excess deposition of coating components during the LbL fabrication process. The multilayer coating that was derived from the reaction mixture of BPEI and 5Acl with 1:10 (v/v) volume ratio provided a multilayer coating—without blocking the available pores of NF as confirmed from the FESEM images in Figure 1B. The deposited multilayer coating was found with randomly aggregated granular domains (average size of about 400 nm; Figure 1B). Further, the elemental mapping analysis confirmed the uniform deposition of porous coatings across the entire substrate (Figure S3, Supporting Information).

The optimized multilayer coating was found to be comprised of residual acrylate groups, as confirmed by Attenuated total reflectance-Fourier transform infrared spectroscopy (ATR-FTIR) in Figure 1D, where the IR signatures for C=O stretching and the deformation of vinylic C–H appeared peak at 1730 cm^{-1} and 1408 cm^{-1}, respectively. On the other side, the XPS analysis confirmed the presence of residual reactive amine groups in the prepared RMC (Figure S4, Supporting Information). These residual acrylate and amine groups were strategically and independently modified to achieve single and dual-modified multilayer coatings with appropriately selected small molecules through the 1,4-conjugate addition reaction at ambient conditions. To prepare different single modified coatings (SMC), the RMC on NF was separately reacted with selected primary amine-containing small molecules, i.e., glucamine (Glu, neutral), β-alanine (β-ala, anionic) and N, N-dimethylaminopropylamine (DMAPA, cationic) through 1,4-cojugate addition reaction and the resulted coatings were denoted as SMC-1, SMC-2, and SMC-3, respectively. The successful post-covalent modifications were characterized with ATR-FTIR analysis, where the characteristic IR signature for vinylic C-H deformation at 1408 cm^{-1} was significantly depleted with respect to the normalized IR peak for carbonyl stretching (Figure 1D). During the 1,4-conjugate addition reaction between residual acrylate groups of prepared RMC and primary amine of selected modifiers, the vinyl group was compromised, and the carbonyl group remained unaffected at the end. Thus, the IR signature for carbonyl group acted as an internal reference to monitor the successful and unambiguous post-covalent modification of the prepared RMC. Thereafter, to derive different dual modified coatings (DMC), these SMCs were separately treated with various acrylate containing small molecules, i.e., 2-hydroxyethyl acrylate (neutral), 3-sulfopropylacrylate (sulfonate acrylate, anionic), 2-(dimethylamine) ethyl acrylate (DMAEA, cationic). Depending on the successive and selective chemical modifications, these coatings were referred as DMC-1 (Glu/hydroxy acrylate), DMC-2 (β-ala/sulfonate acrylate), DMC-3 (DMAPA/sulfonate acrylate) and DMC-4 (DMAPA/DMAEA), where residual amine of the prepared coatings reacted with acrylate groups of selected modifiers through 1,4-conjugate addition reaction. The modification was characterized by ATR-FTIR analysis, as shown in (Figure S5, Supporting Information).

2. Tailoring the Force of Nucleated Hydrogen Bubble Adhesion.

Thereafter, the impact of both single and dual modifications of the prepared RMC on both the water (in air) and air-bubble (underwater) wettability was examined in detail (Figure 1E-F and Figure S6, Supporting Information). The water wettability of the NF altered from hydrophobicity (water contact angle (WCA) of 124.6 ± 1.2°, Figure 1G) to hydrophilicity (WCA of 74.2 ± 0.7°, Figure 1G) on deposition of the RMC—and it became superhydrophilic

with water contact angle of 0° on adaptation of either single or dual modifications—irrespective of the types (neutral, cationic and anionic) of the selected hydrophilic modifiers (Figure 1G). This can be attributed to the introduction of high surface free energy on the porous RMC coating (Figure 1B)—through post-covalent modification with selected hydrophilic molecules. An elevation of surface free energy was observed on modification of RMC with selected modifiers, as shown in Figure 1G (blue dotted line). As a result, WCA was dropped to 0° (Figure 1G)—and the modified coating became superhydrophilic. Interestingly, underwater air bubble contact angle (BCA) of the prepared coatings was noticed to be improved—depending on the selection of single modifiers, i.e., glu (SMC-1; BCA of 145.5 ± 0.3°), β-ala (SMC-2; BCA of 146.9 ± 0.2°) and DMAPA (SMC-3; BCA of 149.1 ± 0.3°) as shown in Figure 1G—however these single modified coatings remained inappropriate to display superaerophobicity as the underwater BCA remained < 150°. On the contrary, the dual modified coatings, i.e., DMC-1, DMC-2, DMC-3, and DMC-4 displayed underwater superaerophobicity with BCA of > 150°, where DMC-4 displayed maximum air-bubble repellence, i.e., 161.1 ± 1.4° as shown in Figure 1F. This elevation of BCA was noticed with increase in the surface free energy (blue dotted line) of the modified coating (Figure 1G; gray bars). The improved hydration of the porous coating becuase of high surface free energy in the submerged condition minimizes the contact between air bubble and prepared coating—and provides extreme bubble repellence. This study revealed that all superhydrophilic interfaces are not adequate to display superaerophobicity—rather, the controlled post-covalent modification tailors the underwater superaerophobicity with distinct underwater air BCA (denoted as θ_a). It is known that θ_a and WCA in air (θ_w), sum up to 180° as they are supplementary to each other.[36,37,38] However, the current approach allowed us to derive a series of highly porous superhydrophilic interfaces ($\theta_w \sim 0°$) that displayed distinct variations in air-bubble contact angles—depending on the selected chemical modifications. This is an unnatural tendency in wetting.

To further understand this unusual gas-bubble wetting behavior, we plot in Figure 1H-I, the wetting diagram of the coated NF with different chemical modifications, in which we obtained the linear relationship that the apparent air BCA increases with the Young contact angle. In this plot, we just changed the chemical modifications of the coating, keeping its structure intact. Thus, it is expected that the plot can be fitted with the Cassie−Baxter model:

$$\cos\theta_a = \varphi\cos\theta_Y - (1-\varphi) \quad (1)$$

where φ is the solid−bubble contact fraction or Wenzel model:

$$\cos\theta_a = r\cos\theta_Y \quad (2)$$

where r is surface roughness.[39] In these models, the intercept of $\cos\theta_a$-axis is always negative or zero. However, the linear fitting we obtained from the plot is following the equation:

$$\cos\theta_a = 2.50\cos\theta_Y + 0.87 \quad (3)$$

with fitting reliability of $R^2 = 0.95$, which can be explained by neither the classical wetting model[36,37,38] nor recently proposed models. [40,41,42]

We have selected DMC-4, having maximum underwater BCA to study HER performance. Thereafter, the stability of the DMC-4 was examined, exposing to various chemically harsh conditions—including extremes of pH, ionic surfactants contaminated (1 mM) aqueous phase, high salinity (5 M) and artificial seawater. The superaerophobicity of DMC-4 remained unaffected even after prolonged (30 days, Figure 2A) exposure to these chemically harsh conditions. Most importantly, the current approach of single and dual-modifications of RMC allowed to modulate force of adhesion of air-bubble underwater. On the association of DMC-4 on NF, the force of adhesion of beaded air-bubble (5 µL) reduced (4.6 ± 0.3 µN) by ~ 96% compared to the bare NF (148.9 ± 2.6 µN), as shown in Figure 2B-C. Interestingly, the selected chemical (single or dual) modifications provided a distinct force of adhesion for a beaded air bubble, as shown in Figure 2B. The force of air bubble adhesion was noticed to be depleted with elevation of the surface free energy of the differently modified coatings, as shown in Figure 2B. This is due to improved hydration of the modified porous coating, where the change in surface free energy because of the difference in the chemical modification controls the extent of hydration of the prepared polymeric coating. Next, an air bubble was beaded and squeezed against the bare and coated (DMC-4) NF, prior to receding the beaded air bubble from respective substrates underwater. We noticed a significant distortion of the air bubble on bare NF during the receding process, even the air bubble was found to be broken and a trace of air bubble remained on the bare NF. (Figure S7, Supporting Information and Movie 1). Whereas the air bubble left the coated NF, neither having any noticeable distortion nor leaving any trace of remnant air bubble on the coated NF (Movie 1). This result independently supports the existence of low force of air-bubble adhesion. The chemically modulated low force of underwater air-bubble adhesion is anticipated to facilitate an early detachment of tiny air-bubbles from the coated electrode. As presented in Figure 2D, hydrogen gas bubbles are generated on the cathode during the electrolysis of water, then they grow into a bigger gas bubble—and block the active catalytic site before leaving the electrode surface. The detachment of the generated gas bubbles on the bare electrode—entirely depends on the two competing forces acting on the generated hydrogen gas bubble underwater, i.e., 1) force of bubble adhesion on the electrode and 2) buoyancy force (Figure 2D). In this section, we

attempted to study the nucleated hydrogen bubble adhesion property of the modified multilayer coating. In this context, we examined the relationship between air bubble adhesion and nucleated hydrogen bubble removal property. This is because the mechanics of the static air bubble adhesion differs from that of nucleated hydrogen bubbles (Figure 2E).[43] In the static air bubble adhesion regime, the single air bubble is attached to the outermost surface of the electrode (Figure 2C). While, the nucleated hydrogen bubbles must exist inside the porous structure of the electrode (Figure 2F). We first measured the buoyancy force applied to the nucleated hydrogen bubble just detached from the surface F_b, which is given by

$$F_b = \frac{\pi D^3(\rho_w - \rho_h)g}{24}[4 - (1 + \cos\theta_h)^2(2 + \cos\theta_h)] \text{ for } \frac{\pi}{2} < \theta_h < \pi \quad (4)$$

where D, ρ_w, ρ_h, g, and θ_h are bubble departure diameter, water density, hydrogen density, gravitation acceleration constant, and hydrogen bubble contact angle. We estimated that the hydrogen BCA is equal to that of air (that is $\theta_a \approx \theta_h$) and quantified F_b. Figure 2G shows that F_b is linearly proportional to F_a, which fills the gap between the air bubble adhesion and nucleated hydrogen bubble removal property. Moreover, F_b is balanced with the adhesion force of the nucleated hydrogen bubble, F_h (Figure 2E), which is estimated by the Young-Dupré model, which yields:[44]

$$F_h = \pi D \gamma_{w'} \cos\theta_h \ (1 + \cos\theta_h) \quad (5)$$

where $\gamma_{w'}$ is water–hydrogen interfacial tension. We assumed $\gamma_{w'} \approx \gamma_w$ and obtained the relationship between $F_h \sim F_b$ (Figure 2H). The net force between F_h and F_b maybe the viscous energy dissipation force in hydrogen bubble growth. Further, we estimated Eötvös number Eo, which is a dimensionless quantity representing the relative effect of buoyancy forces versus capillary forces, given by

$$\text{Eo} = (\rho_w - \rho_h) g D^2 \gamma_{w'}^{-1} \quad (6)$$

Figure 2I shows the effect of the chemical modification on D and Eo. When the surface is bare, the bubble departure diameter is large enough to work buoyancy force to detach the bubble from the substrate (Eo > 1). However, after the chemical modification, the bubble departure diameter is small to be Eo << 1. Especially, DMC-4 removed the hydrogen bubble with a minimum size of 0.64 mm and Eo = 0.05. It means the chemically modified surface can remove nucleated hydrogen bubbles with negligible buoyancy force. Thus, a tiny (diameter of 0.64 mm) gas bubble was released underwater from coated NF, as shown in Figure 2J. Whereas a significantly larger (~ 4.6 times) gas bubble was noticed to be detached from the bare NF. (Figure 2K). We noticed a depletion in the size of detached gas-bubbles from coated NF—depending on the selection of post modifications. (Figure S8, Supporting Information). The

larger gas bubbles attached on bare NF lead to a high electrode surface coverage during electrolysis, and eventually, it is likely to reduce electrolyte diffusion and increase polarization loss—which eventually compromises the HER performance.

Notably, the electrochemically generated bubbles are first entrapped in the topography, corresponding to the Wenzel state, where the easy detachment of these bubbles is difficult for conventional interfaces. However, in our case, these bubbles detached with extremely small diameters, indicating that our chemical modulation has a high hydration ability on the surface, enough to cause a transition from Wenzel to Cassie state. This excellent hydration ability is supported by the data: (1) well-matched probe-bubble adhesion force vs. generated-bubble adhesion force (Figure 2G-H, and (2) unclassical wettability diagram Young contact angle vs. apparent contact angle (Figure 1I). Generally, to increase the electrode efficiency, increasing the surface roughness (area) is promising; however, the adhesion force of the nucleated hydrogen bubble should be increased with the surface roughness, leading to a decrease in the electrode efficiency. While the smooth hydrophilic coating, for example, hydrogel coating, enabled superaerophobicity,[27] our coating gives the electrode both nanoscale roughness and excellent hydrogen bubble removal property.

3. Influence of Tailored Force of Air-Bubble Adhesion on HER Performance.

In the following section, we have examined and compared the HER performance of NF (utilized as a working electrode in a three-electrode setup) with and without single and dual modified coatings under alkaline condition (1M aq. KOH, pH 14), where no additional electrocatalysts were involved. The HER performance was significantly improved on the association of both single-modified (SMC-1, SMC-2, SMC-3) and dual-modified (DMC-1, DMC-2, DMC-3, DMC-4) coatings; however, DMC-4 exhibited highest current density of -1270 mA cm^{-2} at -0.9 V versus reversible hydrogen electrode (RHE), which is almost double than that of the bare NF (-680 mA cm^{-2}) (Figure 3A). This can be attributed to the early detachment of generated hydrogen gas bubbles, as evident from the digital images in Figure 3B, where smaller gas bubbles left the coated (DMC-4) electrode surface in comparison to the bare electrode (Figure 3B). Further, Movie 2 allows to directly visualize the difference in the sizes of detached hydrogen gas bubbles from bare and coated (DMC-4) NF electrodes at a current density of 500 mA cm^{-2}. This current strategy improved the overpotential of HER at both low and high current densities (Figure 3C). Notably, the NF electrode coated with DMC-4 displayed a depleted overpotential for HER at low current density of 100 mA cm^{-2} than those reported coatings embedded with additional catalysts.[27, 29, 30] This is because the generated gas bubbles are

expected to be attached more firmly on the bare or conventional electrode surface at low current. At the low current density, the generation of gas bubbles is less, hence the growth of the gas bubble will be slow, and it would be challenging to acquire enough size and buoyancy force to compensate the high force of bubble adhesion on bare NF. Eventually, the blockage of the bare NF because of nucleated bubble is more prominent in low current density as clearly demonstrated in Movie 3. On the other hand, the chemically modified coating (DMC-4) embedded with low force of bubble adhesion enabled early detachment of the nucleated hydrogen bubbles even at low current density of 10 mA cm^{-2} as shown in Movie 3. Thus, even at very low current density, the currently prepared coating remained effective to keep the overpotential low and displayed a superior HER performance compared to relevant literature (Scheme 1E).

The overpotential at a high current density of −500 mA cm^{-2} was also decreased from -748 mV (of bare NF) to -512 mV (Figure 3C) for coated (DMC-4) NF. Whereas the other dual-modified coatings, i.e., DMC-1, DMC-2 and DMC-3, showed a relatively lesser change in overpotential values, i.e., -598, -596 and -576 mV, respectively. To understand the role of superaerophobicity with modulated force of bubble adhesion on this improved electrochemical HER performance, we have performed a control experiment to compare the LSV trace of bare NF and NF with RMC—prior to its post-covalent modifications with desired modifiers. A very similar electrochemical performance (current density of 658 mA cm^{-2} at the potential of -0.9 (Vs HER) and overpotential of 760 mV at current density of -500 mA cm^{-2}) was noticed for the NF with RMC when compared with bare NF, as shown in Figure 3A, C. However, the RMC on NF, which was subjected to appropriate post-covalent modifications (SMC/DMC) for conferring superaerophobicity with the modulated force of bubble adhesion, displayed a significant improvement in HER performance (with respect to current density and overpotential; Figure 3A, C). In another separate control study, RMC was modified with ODA to acheive an underwater superaerophilicity with BCA of 0°—and such superaerophilic coating on NF displayed a poor HER performance when compared with bare NF (Figure S9, Supporting Information).These control studies unambiguously support that the current strategy of chemically modulated tailoring of force of adhesion of gas bubble provided a simple basis to improve current density and overpotential of HER – through the early detachment of gas bubbles. The low force of nucleated hydrogen gas bubble adhesion (4.6 ± 0.3 μN) of DMC-4—which enables the detachment of generated tiny hydrogen gas bubbles—helped to reduce “dead space” on the electrode surface during HER and improved micro-convection of electrolyte.

Eventually, the overpotential was observed to be depleted (Figure 3C) even at a high (−500 mA cm^{-2}) current density. Thus, negligible or no involvement of intrinsic catalytic activity of deposited multilayer coating embedded with modulated force of bubble adhesion is expected towards the improved HER performance. Notably, as the applied current density increased, the difference between the required potential for the bare NF and DMC-4 coated NF electrodes became larger as more hydrogen bubbles were formed and adhered to the bare electrodes at higher current densities. These findings showed the importance of lowering the force of nucleated hydrogen gas bubbles to address the bubble detachment challenge.

Thereafter, the Tafel slope of NF electrode with and without DMC-4 was measured from the steady-state polarization curve following reported protocol,[45] and a minimal change (157.8 vs 162.9 mV dec^{-1}) in the slope values was noticed—which suggests that DMC-4 had a negligible influence on the water splitting mechanism of the selected native electrode (i.e., NF, Figure 3D).[46] This implied that the current strategy of chemically modulated tailoring of the force of adhesion of gas bubble has the ability to improve the overpotential for HER activity without affecting the HER mechanism of the native electrodes. To provide more insights into the role of DMC-4 on HER performance, electrochemical impedance spectroscopy (EIS) data was investigated at -0.25 V vs. RHE. [27,47-48] The decrease in both series resistance (R1) and charge transfer resistance (R2) was observed when the bare NF electrode was coated with DMC-4 (Figure 3E). This is because of the early detachment of nucleated hydrogen gas bubbles on the coated (DMC-4) NF electrode. The attachment of big gas bubbles on bare NF electrode reduces effective surface area and increases resistance of the electrode (Figure 3E). Moreover, LSV curves for bare and coated (DMC-4) electrodes with and without iR corrections are provided in Figure 3F. After the iR corrections, bare and coated (DMC-4) electrodes displayed similar polarization curves (Figure 3F). This result also suggested that the improved HER performance of the coated electrode is because of the lower resistance of the coated electrode with respect to the bare electrode.[27] The bare electrode suffers from the blockage of the catalytic surface because of the bubble attachment—and lead to elevation in resistance of bare NF. Thereafter, electrochemically active surface area (ECSA) was analyzed. The active surface area of bare NF and coated (DMC-4) NF electrodes were 1.3 and 1.1 mF cm^{-2} (Figure 4A), (Figure S10, Supporting Information). This slight decrease in ECSA implied partial blocking of active sites in coated (DMC-4) NF. However, the embedded superaerophobicity with low force of bubble adhesion in coated (DMC-4) NF facilitates detachment of generated tiny gas bubbles—and prevents further blockage of the active surface area of the electrode during HER

at low and high current densities. However, unavoidable blockage of the catalytic surface area in bare electrode because of the large bubble attachment—restricts the access of electrolytes—and enhances the ionic resistance during HER.

To further check the stability of the coated (DMC-4) NF electrode for practical application, a chronoamperometric stability test was performed. Chronoamperometric data was recorded at a current density of -250 mA cm^{-2}. A slight depletion in current density (245 mA cm^{-2}) was noticed after 60 h (Figure 4B), which suggests the stability of coated electrode. Moreovere, there was a negligible change in the LSV traces before (red solid line in Figure 4C) and after (black solid line in Figure 4C) the stability test, further confirming the stability of the coated (DMC-4) electrodes. Furthermore, the superaerophobicity of the coated (DMC-4) electrode remained intact with an air BCA of ~160° (Figure 4D) and force of adhesion of 5.3 ± 0.5 μN even after performing chronoamperometric stability for 60 h (Figure 4E). The deconvoluted XPS spectra (Figure S11, Supporting Information), FESEM images (Figure S12 A-B, Supporting Information), and FTIR spectra (Figure S12C, Supporting Information) independently support the stability of the coated NF. The coated (DMC-4) NF electrode before and after exposing it to harsh chemical environments for 1 month (Figure 2A) displayed very similar polarization curves and Tafel slopes for HER (Figure S13, Supporting Information).

Finally, electrolysis was carried out in two-electrode mode employing coated (DMC-4) NF as the cathode and bare NF as an anode to replicate the electrolyzer configuration. While the theoretically required voltage for overall water splitting is 1.23 V, the experimentally required voltage for water splitting in this 2 electrode set-up is observed to be 2.14 V at current density of 100 mA cm^{-2} (Figure 4F). Hence, the overpotential for overall water splitting in 2 electrode system was calculated to be 910 mV (at current density of 100 mA cm^{-2})—which matches well when compared with the combined overpotential of individual OER (650 mV) and HER (250 mV)—which are calculated using 3 electrode electrolyzer configuration. The faradaic efficiency of H_2 production was calculated by comparing the theoretical and experimental values using earlier reported procedures in two electrode system.[49-50] The faradaic efficiency for H_2 was estimated to be ~ 98.2% (Figure S14, Supporting Information). The HER faradaic efficiency remained constant over the course of the run, indicating that the electrode material is sufficiently stable. To further check the universality of our approach, other electrodes, such as carbon cloth and carbon paper electrodes, were also coated with DMC-4 prior to examining their HER performance (Figure 4G and Figure S15, Supporting Information). The result suggests that the current chemical modification approach to modulate the force of

nucleated hydrogen gas bubble adhesion has immense potential to improve the HER performance of different electrodes.

Conclusion

In brief, the performance of multilayer coated electrodes in the alkaline hydrogen evolution reaction can be notably enhanced by tailoring the force of nucleated hydrogen gas bubble adhesion underwater—without associating additional electrocatalysts or complex and specific fabrication processes. By adjusting the formulation of the multilayer coatings—and followed by strategic post modifications, we could regulate the porosity, aerophobicity, and force of nucleated hydrogen gas bubble adhesion—which attributed to improved HER activity. The NF electrode coated with DMC-4 displayed superior performance compared to other single/dual modified coatings and existing literature, particularly at high current densities, due to its ability to swiftly eliminate tiny nucleated hydrogen gas bubbles from the electrode surface. Moreover, this strategy can be successfully applied on other electrodes to achieve improved HER performance. Our current findings provide important insights into designing efficient electrodes for HER—without associating additional state of the art catalysts and open doors for the practical implementation of water electrolysis and green energy production.

References

[1] Y. Zhang, K. E. Arpino, Q. Yang, N. Kikugawa, D. A. Sokolov, C. W. Hicks, J. Liu, C. Felser, G. Li, *Nat. Commun.* **2022**, *13*, 7784.

[2] H. Zhao, Z. Y. Yuan, *Adv. Energy Mater.* **2023**, *13*, 2300254.

[3] J. Guo, Y. Zheng, Z. Hu, C. Zheng, J. Mao, K. Du, M. Jaroniec, S. Qiao, T. Ling, *Nat. Energy* **2023**, *8*, 264–272.

[4] C. Deng, C. Y. Toe, X. Li, J. Tan, H. Yang, Q. Hu, C. He, *Adv. Energy Mater.* **2022**, *12*, 2201047.

[5] K. Maiti, S. Maiti, M. T. Curnan, H. J. Kim, J. W. Han, *Adv. Energy Mater*. **2021**, *11*, 2101670.

[6] J. Su, Y. Yang, G. Xia, J. Chen, P. Jiang, Q. Chen, *Nat. Commun*. **2017**, *8*, 14969.

[7] M. Wang, X. Zheng, D. Qin, M. Li, K. Sun, C. Liu, W.-C. Cheong, Z. Liu, Y. Chen, S. Liu, B. Wang, Y. Li, Y. Liu, C. Liu, X. Yang, X. Feng, C. Yang, C. Chen, Y. Pan, *Small* **2022**, *18*, 2201974.

[8] P. Zhang, K. Chen, J. Li, M. Wang, M. Li, Y. Liu, Y. Pan, *Adv. Mater.* **2023**, *35*, 2303243.

[9] Y. Pan, X. Ma, M. Wang, X. Yang, S. Liu, H.-C. Chen, Z. Zhuang, Y. Zhang, W.-C. Cheong, C. Zhang, X. Cao, R. Shen, Q. Xu, W. Zhu, Y. Liu, X. Wang, X. Zhang, W. Yan, J. Li, H. M. Chen, C. Chen, Y. Li, *Adv. Mater.* **2022**, *34*, 2203621.

[10] M. Li, H. Zhu, Q. Yuan, T. Li, M. Wang, P. Zhang, Y. Zhao, D. Qin, W. Guo, B. Liu X. Yang, Y. Liu, Y. Pan, *Adv. Funct. Mater.* **2023**, *33*, 2210867.

[11] M. Wang, K. Sun, W. Mi, C. Feng, Z. Guan, Y. Liu, Y. Pan, *ACS Catal.* **2022**, *12*, 10771−10780.

[12] C. Zhang, Z. Xu, N. Han, Y. Tian, T. Kallio, C. Yu, L. Jiang, *Sci. Adv.* **2023**, *9*, eadd6978.

[13] H. Vogt, *J. Electrochem. Soc.* **1990**, *137*, 1179–1184.

[14] J. Dukovic, C. W. Tobias, *J. Electrochem. Soc.* **1987**, *134*, 331–343.

[15] C. Gabrielli, F. Huet, R. P. Nogueira, *Electrochim. Acta* **2005**, *50*, 3726–3736.

[16] Y. Kang, S. Lee, S. Han, D. Jeon, M. Bae, Y. Choi, D. W. Lee, J. Ryu, *Adv. Funct. Mater.* **2023**, 2308827.

[17] M. S. Faber, R. Dziedzic, M. A. Lukowski, N. S. Kaiser, Q. Ding, S. Jin, *J. Am. Chem. Soc.* **2014**, *136*, 10053–10061.

[18] H. Cheng, K. Scott, C. Ramshaw, *J. Electro.chem. Soc.* **2002**, *149*, D172 -D177.

[19] S. D. Li, C. C. Wang, C. Y. Chen, *Electrochim. Acta* **2009**, *54*, 3877–3883.

[20] T. Iida, H. Matsushima, Y. Fukunaka, *J. Electrochem. Soc.* **2007**, *154*, E112.

[21] L. Wang, X. Duan, X. Liu, J. Gu, R. Si, Y. Qiu, Y. Qiu, D. Shi, F. Chen, X. Sun, J. Lin, J. Sun, *Adv. Energy Mater*. **2020**, *10*, 1903137.

[22] X. Yu, Z. Y. Yu, X. L. Zhang, Y. R. Zheng, Y. Duan, Q. Gao, R. Wu, B. Sun, M. R. Gao, G. Wang, S. H. Yu, *J. Am. Chem. Soc.* **2019**, *141*, 7537–7543.

[23] R. Andaveh, B. Darband, M. Maleki, A. S. Rouhaghdam, *J. Mater. Chem. A* **2022**, *10*, 5147–5173.

[24] Z. Lu, W. Zhu, X. Yu, H. Zhang, Y. Li, X. Sun, X. Wang, H. Wang, J. Wang, J. Luo, X. Lei, L. Jiang, *Adv.Mater.* **2014**, *26*, 2683–2687.

[25] Y. Li, H. Zhang, T. Xu, Z. Lu, X. Wu, P. Wan, X. Sun, L. Jiang, *Adv. Funct. Mater.* **2015**, *25*, 1737–1744.

[26] J. Y. Zhang, J. Liang, B. Mei, K. Lan, L. Zu, T. Zhao, Y. Ma, Y. Chen, Z. Lv, Y. Yang, C. Yu, Z. Xu, B. Y. Xia, W. Li, Q. Yuan, D. Zhao, *Adv. Energy Mater.* **2022**, *12*, 2200001.

[27] M. Bae, Y. Kang, D. W. Lee, D. Jeon, J. Ryu, *Adv. Energy Mater.* **2022**, *12*, 2201452.

[28] D. Jeon, J. Park, C. Shin, H. Kim, J. W. Jang, D. W. Lee, J. Ryu, *Sci. Adv.* **2020**, *6*, eaaz3944.

[29] P. W. Menezes, C. Panda, S. Loos, F. Bunschei-Bruns, C. Walter, M. Schwarze, X. Deng, H. Dau, M. Driess, *Energy Environ. Sci.* **2018**, *11*, 1287–1298.

[30] L. Wang, X. Duan, X. Liu, J. Gu, R. Si, Y. Qiu, Y. Qiu, D. Shi, F. Chen, X. Sun, J. Lin, J. Sun, *Adv. Energy Mater.* **2020**, *10*, 1903137.

[31] J. J. Richardson, M. Björnmalm, F. Caruso, *Science* **2015**, *348*, aaa2491.

[32] S. Zhao, F. Caruso, L. Dähne, G. Decher, B. G. De Geest, J. Fan, N. Feliu, Y. Gogotsi, P. T. Hammond, M. C. Hersam, A. Khademhosseini, N. Kotov, S. Leporatti, Y. Li, F. Lisdat, L. M. Liz-Marzán, S. Moya, P. Mulvaney, A. L. Rogach, S. Roy, D. G. Shchukin, A. G. Skirtach, M. M. Stevens, G. B. Sukhorukov, P. S. Weiss, Z. Yue, D. Zhu, W. J. Parak, *ACS Nano* **2019**, *13*, 6151–6169.

[33] D. Jeon, H. Kim, C. Lee, Y. Han, M. Gu, B. S. Kim, J. Ryu, *ACS Appl. Mater. Interfaces* **2017**, *9*, 40151–40161.

[34] A. Borbora, R. L. Dupont, Y. Xu, X. Wang, U. Manna, *Mater. Horiz.* **2022**, *9*, 991–1001.

[35] D. Parbat, U. Manna, *Chem. Sci.* **2017**, 8, 6092-6102.

[36] X. Tian, V. Jokinen, J. Li, J. Sainio, R. H. A. Ras, *Adv. Mater.* **2016**, *28*, 10652–10658.

[37] Y. Zhao, Z. Xu, L. Gong, S. Yang, H. Zeng, C. He, D. Ge, L. Yang, *iScience* **2021**, *24*, 103427

[38] Y. Kaufman, S. Y. Chen, H. Mishra, A. M. Schrader, D. W. Lee, S. Das, S. H. Donaldson, J. N. Israelachvili, *J. Phys. Chem. C* **2017**, *121*, 5642−5656.

[39] A. Lafuma, D. Quéré, *Nat. Mater.* **2003**, *2*, 457–460.

[40] H. C. Kang, A. M. Jacobi, *Langmuir* **2011**, *27*, 14910–14918.

[41] A. Tuteja, W. Choi, J. M. Mabry, R. E. Cohen, *Proc. Natl. Acad. Sci. U.S.A.* **2008**, *105*, 18200.

[42] K. L. Wilke, Z. Lu, Y. Song, E. N. Wang, *Proc. Natl. Acad. Sci. U.S.A.* **2022**, *119*, e2109052119.

[43] J. L. Liow, N. B. Gra, *Chem. Engg. Science* **1988**, *43*, 3129–3139.

[44] I. You, T. G. Lee, Y. S. Nam, H. Lee, *ACS Nano* **2014**, *8*, 9016–9024.

[45] S. Anantharaj, S. Noda, M. Driess, P. W. Menezes, *ACS Energy Lett.* **2021**, 6, 4, 1607–1611.

[46] J. Durst, A. Siebel, C. Simon, F. Hasché, J. Herranz, H. A. Gasteiger, *Energ. Environ. Sci.* **2014**, *7*, 2255–2260.

[47] S. Anantharaj, S. Noda, *ChemElectroChem*. **2020**, *7*, 2297-2308.

[48] A. J. Bard, L. R. Faulkner, Electrochemical Methods: Fundamentals and Applications, *Wiley-Interscience Publications*, **2000**.

[49] A. Tewary, S. Mandal, Z. Alam, A. S. K. Sinha, U. Ojha, *ACS Sustainable Chem. Eng.* **2023**, *11*, 6556–6566.

[50] L. Ji, J. Wang, X. Teng, T. J. Meyer, Z. Chen, *ACS Catal.* **2020**, *10*, 412–419.

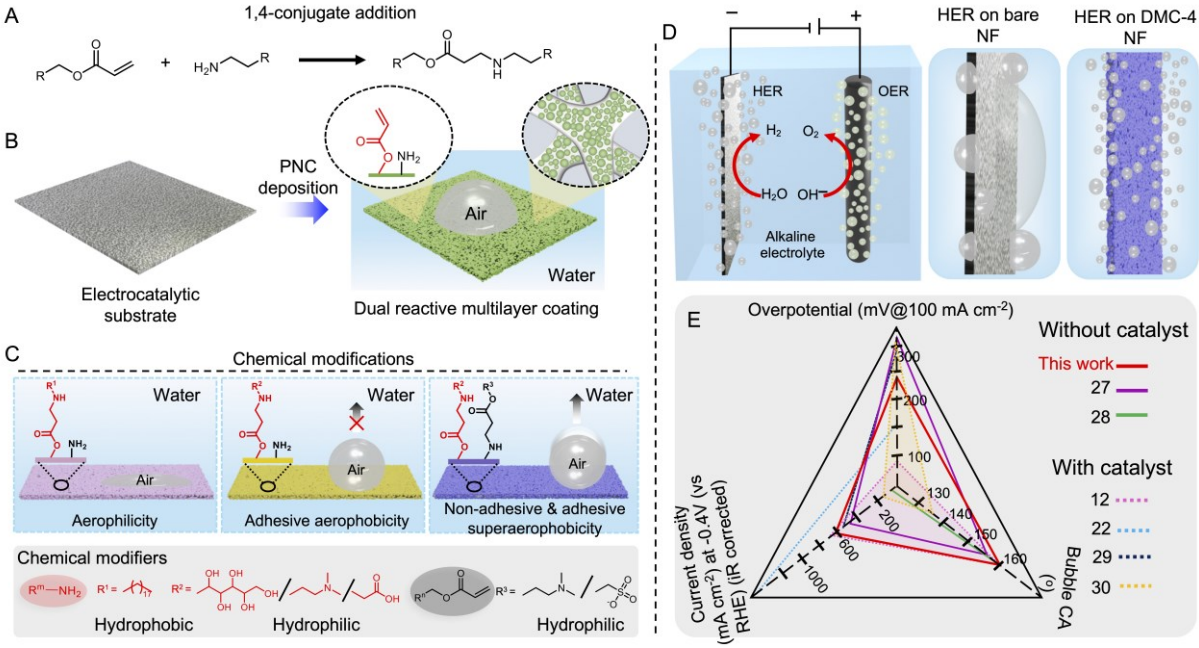

Scheme 1. (A) Accounting 1,4-conjugate addition reaction between representative acrylate and amine groups. B) Schematic depicting the deposition of chemically reactive multilayer coating comprised of residual acrylate and amine on a selected electrode (nickel foam, NF). C) Schematic illustration for chemical modification of reactive multilayer coating deposited on NF with different chemical modifiers to impart different types of underwater air bubble wettability—aerophilicity, aerophobicity and adhesive/non-adhesive superaerophobicity. (D) Schematic depicting electrochemical setup for HER, where hydrogen gas bubbles generation on bare NF and coated (DMC-4) NF is compared. While the bare NF surface was covered with larger hydrogen gas bubbles, the coated (DMC-4) NF remained efficient in detaching generated tiny hydrogen gas bubbles during HER. (E) The spider plot accounting the HER performance

of different electrode systems without (solid line, Ref. [27], [28]) or with (dotted line) additional catalyst (Ref. [12], [22], [29], [30]).

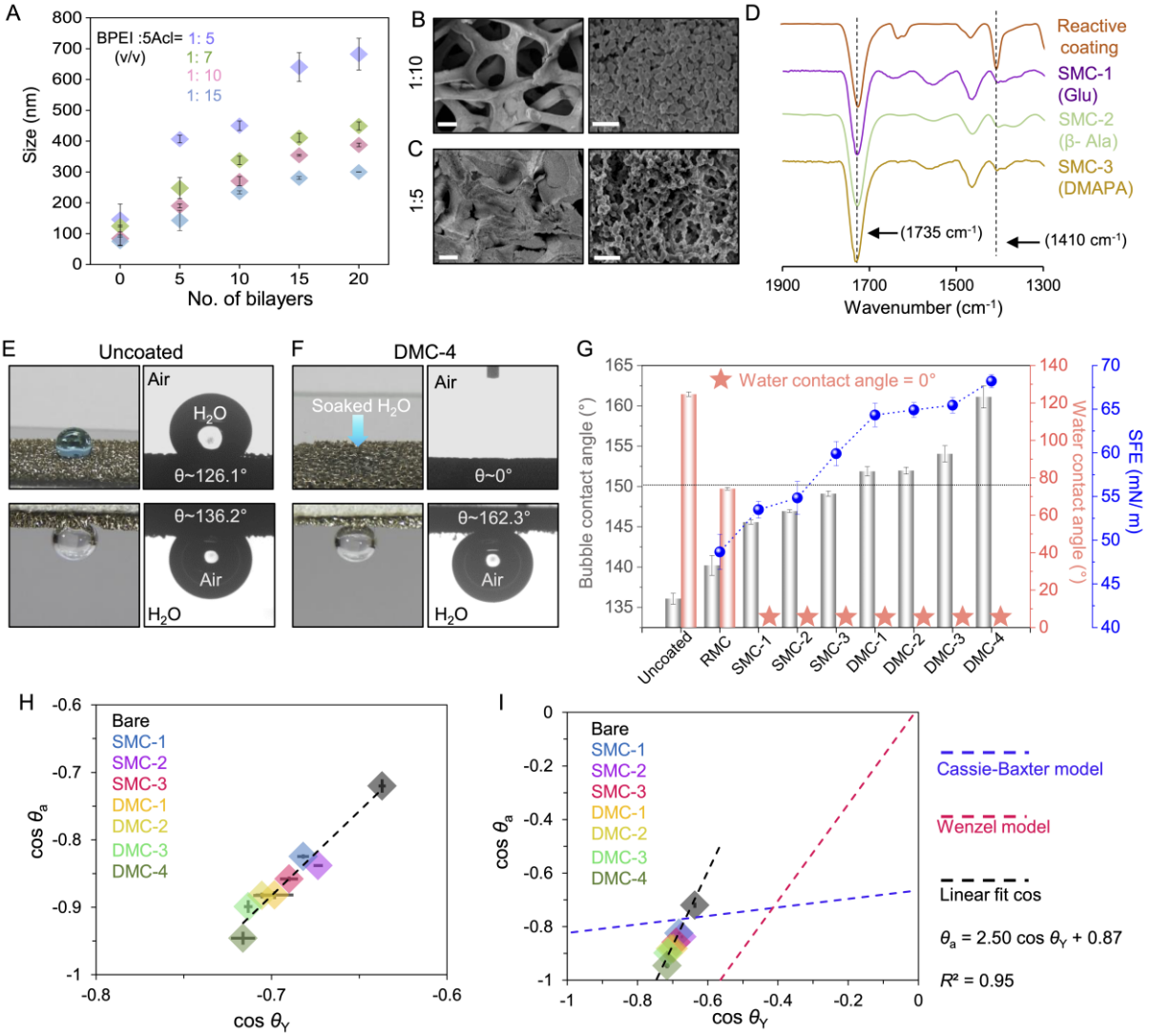

Figure 1: (A) Accounting the growth in the size of the polymeric nanocomplex in dipping solution (prepared by mixing BPEI and 5Acl with different volume ratios) with the number of bilayer depositions. B-C) FESEM images of multilayer coated NF that were derived separately from dipping solutions having volume composition of BPEI (50 mg mL^{-1}) and 5Acl (132.5 mg mL^{-1}) of 1:10 (B) and 1:5 (C) in low (Scale bar, 100 µm; left panel) and high (Scale bar, 1 µm; right panel) magnifications. (D) FTIR spectra of the reactive multilayer coating (RMC) before and after post-covalent modifications with selected modifiers. E-F) Digital and contact angle goniometer images demonstrating wettability of water (in air, top panel) and air-bubble (underwater, bottom panel) on uncoated NF (E) and NF with dual modified coating (DMC-4, F). (G) Illustrating the impact of different single and dual-modifications of RMC on air bubble contact angle (BCA, underwater), water contact angle (WCA, in air), and surface free energy (SFE). (H-I) Wetting diagram representing the relationship between Young contact angle of air

bubble (θ_Y) and air bubble contact angle on coated (SMC/DMC) & bare NF (θ_a). H is magnified and I with classical wetting models: Cassie-Baxter model (blue dotted line) and Wenzel model (red dotted line), and the linear fit of the plot is obtained in this work. Results are presented as mean ± SD, where sample size, n = 3.

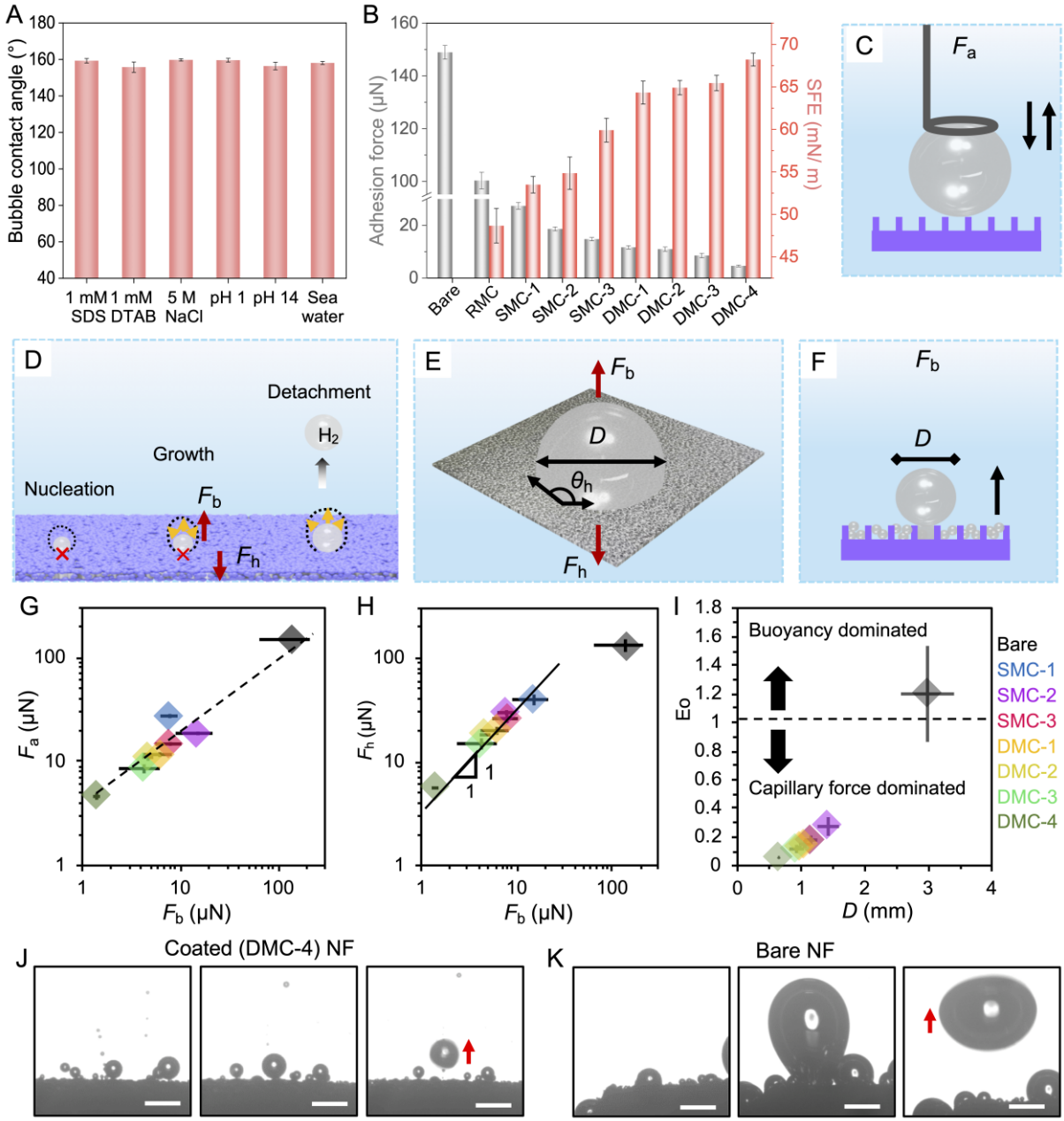

Figure 2. (A) Contact angle mesurments accounting the chemical stability of the embedded superaerophobicity of the DMC-4 at severe and relevant conditions. (B) Depicting the change in force of static bubbles adhesion on the coated (RMC and differently modified (SMC/DMC)) NFs with surface free energy of the coating. (C) Schematic of bulk air bubble adhesion statics on DMC-4 coated NF. (D) Schematic illustrations of hydrogen bubble nucleation, growth and detachment on DMC-4 coated NF. (E) Mechanics of the nucleated hydrogen bubble just in

detachment. F) Illustrating the adhesion of nucleated hydrogen bubbles on DMC-4 coated NF. G-H) Relationship between F_a vs F_b and estimated F_b vs F_h. I) Bubble departure diameter vs. Eötvös number. J-K) Accounting the growth and detachment of (J) tiny nucleated gas-bubble on coated (DMC-4) NF, whereas (K) a larger size of gas-bubble remained attached to the bare NF, where red arrow denotes the detached gas bubble. Scale bar: 1 mm. Results are presented as mean ± SD, where sample size, n = 3.

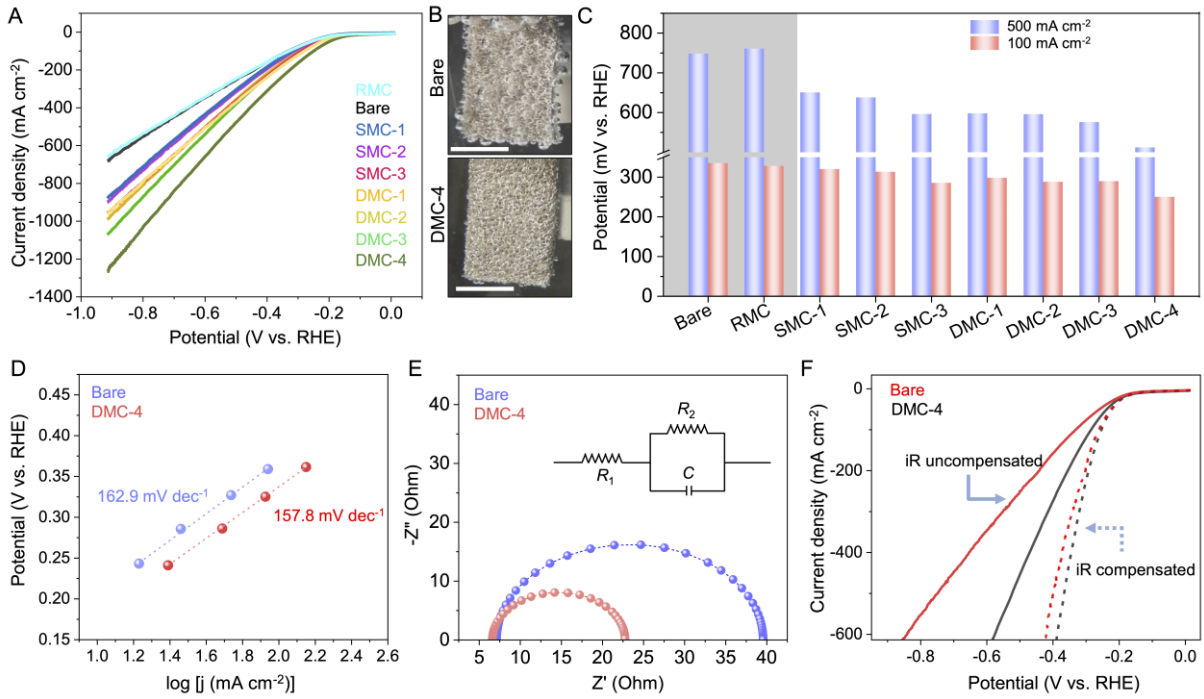

Figure 3. (A) LSV traces of bare NF and NFs—with RMC and differently post-modified (SMC/DMC) coatings. (B) Digital images of bare (top panel) and coated (DMC-4, bottom panel) NF during hydrogen evolution at current density of 500 mA cm^{-2}. (C) Comparison of overpotential of bare NF, RMC-deposited NF and NFs—with differently postmodified (SMC/DMC) coatings at low (100 mA cm^{-2}) and high (500 mA cm^{-2}) current densities. (D) Tafel plot of bare and coated (DMC-4) NF, (E) Nyquist plots of bare and coated (DMC-4) NF, equivalent circuit is presented in the inset, (F) Comparision of LSV traces of bare (red) and DMC-4 coated (black) NF with (dotted line) and without (solid line) iR correction. Results are presented as mean ± SD, where sample size, n = 3.

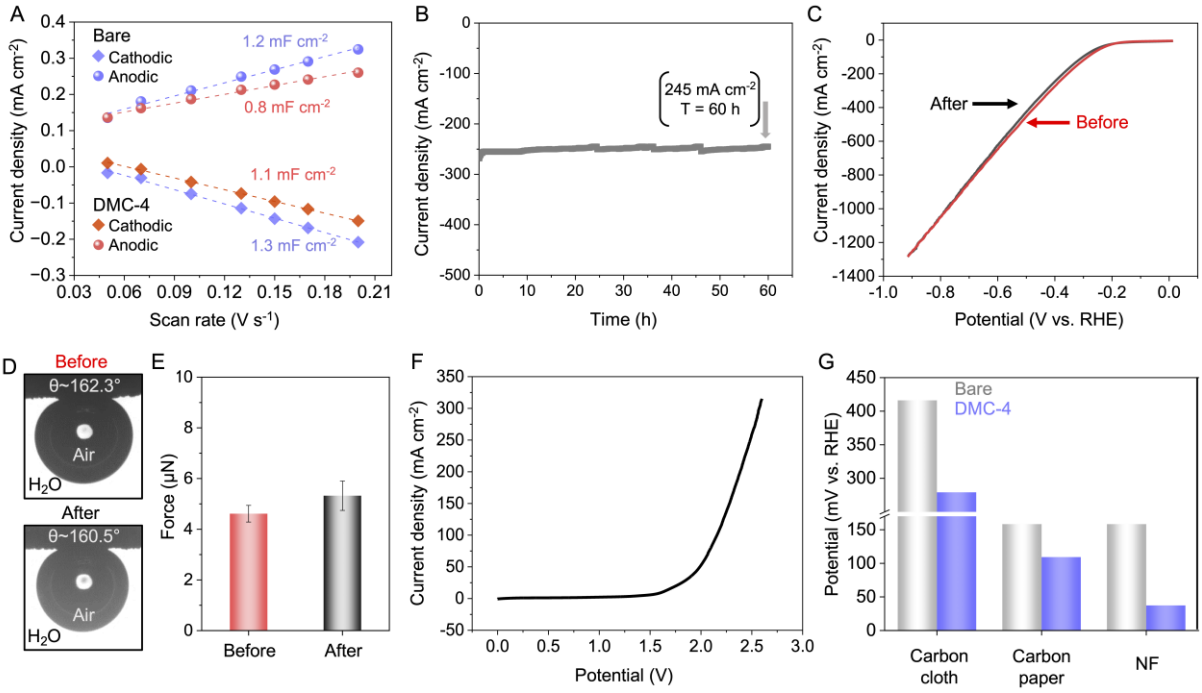

Figure 4. (A) ESCA of bare and coated (DMC-4) NF. (B) Chronoamperometric stability test of coated (DMC-4) NF was performed at current density of 250 mA cm^{-2} and potential of 350 mV for 60 h. (C) LSV traces of coated (DMC-4) NF before (red) and after (black) performing stability test. (D) Contact angle goniometer images depicting the superaerophobicity of the coated (DMC-4) NF before and after stability test for 60 h at current density of 250 mA cm^{-2}. (E) Accounting force of air-bubble adhesion before and after stability test for 60 h at current density of 250 mA cm^{-2} F) LSV trace of coated (DMC-4) NF electrode in two electrode mode. (G) Comparison of HER overpotential of uncoated and coated (DMC-4) carbon cloth, carbon paper, and NF electrodes at current density of 10 mA cm^{-2}. Results are presented as mean ± SD, where sample size, n = 3.

Supplementary information

The online version contains experimental section and supplementary material.

Statistical analysis

All the experiments were performed in triplicates. Results are presented as mean ± SD

Acknowledgments

U.M. thanks Science and Engineering Research Board (CRG/2022/000710), Ministry of Electronics and Information Technology (no. 5(1)/2022-NANO) for financial support. U.M. thanks CIF, CFN, SHST and the Department of Chemistry, Indian Institute of Technology

Guwahati, for their generous assistance in executing various experiments and for the infrastructures. J.D. thanks the UGC and A.B. thanks CSIR for their JRF fellowship. We thank Prof. Mohammad Qureshi, Prof. Uday Narayan Maiti and Mr. Golam Masud Karim for useful discussions.

Conflict of Interest

The authors declare no conflict of interest

Data Availability Statement

The data presented in this article are available from the corresponding authors on reasonable requests.

Table of Contents Entry:

An aerophobic coating having an unprecedented ability to chemically modulate the force of nucleated gas bubbles on electrode surface is prepared following a 1,4-conjugate addition reaction at ambient conditions for improving electrochemical hydrogen evolution reaction (HER), without involving any additional catalyst. The prepared coating enabled a rare capillary force dominated early detachment of nucleated tiny hydrogen bubble—to maintain low overpotential for HER with respect to bare NF.

Keywords: Reactive coating• Chemical modifications • Aerophobicity • Nucleated gas-bubble adhesion • Electrochemical water splitting

Title: Modulating Force of Nucleated Hydrogen Bubble Adhesion to Boost Electrochemical Water Splitting

Jaysri Das[a,§], Subhankar Mandal[b,§], Angana Borbora,[a] Mizuki Tenjimbayashi[d]* Uttam Manna[a,b,c]*